JGR Oceans

RESEARCH ARTICLE
10.1029/2020JC016967

Special Section:
Community Earth System Model version 2 (CESM2) Special Collection

Tropical Pacific Air-Sea Interaction Processes and Biases in CESM2 and Their Relation to El Niño Development

Ho-Hsuan Wei[1,2], Aneesh C. Subramanian[2], Kristopher B. Karnauskas[1,2], Charlotte A. DeMott[3], Matthew R. Mazloff[4], and Magdalena A. Balmaseda[5]

[1]Cooperative Institute for Research in Environmental Sciences, Boulder, CO, USA, [2]University of Colorado, Boulder, CO, USA, [3]Colorado State University, Fort Collins, CO, USA, [4]Scripps Institution of Oceanography, University of California San Diego, La Jolla, CA, USA, [5]The European Centre for Medium-Range Weather Forecasts, Reading, UK

Abstract Coupled processes and associated subsurface dynamics near the eastern edge of the Indo/western Pacific (WP) Warm Pool are important for air-sea interactions involved in tropical Pacific dynamics. We seek to shed light on the physical mechanisms governing air-sea interactions in the region and the impacts of their biases in models. In this study, we use the Ocean ReAnalysis System 5 (ORAS5) to identify mean-state biases in the National Center for Atmospheric Research Community Earth System Model version 2 (CESM2) with a particular focus on upper ocean properties and air-sea interaction processes. We show that the CESM2 has warm and fresh surface biases in the tropical Pacific Ocean, a barrier layer that is too thin in the WP, and an isothermal layer depth (ILD) that is too deep in the eastern Pacific (EP). These biases impact air-sea interaction processes involved in El Niño development. We compare the strong El Niño events in ORAS5 and CESM2 and show that biases in barrier layer thickness in the WP and in ILD in the EP are significant before the onset of the El Niño events. These biases then influence vertical mixing and entrainment processes, resulting in mixed layer cooling biases. Biases in the sea surface temperature seasonal cycle in the CESM2 also influence the development of the El Niño. We emphasize how the El Niño progression in models can be influenced by its sensitivity to the mean state biases in both subsurface ocean structure and seasonal cycle through local as well as the large-scale physical processes.

Plain Language Summary The western tropical Pacific has warm ocean surface temperatures that extend to over 100 m depth due to the prevailing trade winds. In contrast, the eastern tropical Pacific has cold ocean surface temperatures due to the upwelling of cold water from below. Changes to the trade winds can lead to changes in these temperatures and the whole ocean-atmosphere coupled system. We shed light on the important physical processes that govern the ocean-atmosphere interactions in the western tropical Pacific and how models have limitations in representing some of the processes, which potentially leads to errors in the simulation of important climate events such as El Niño. We show that the Community Earth System Model, a widely used global climate model, has warmer and fresher ocean surface waters compared to observations in this region which then influences the ocean-atmosphere interactions adversely in this region. We also show that the so-called "barrier" layer, which restricts the cold, deep water from reaching the surface when mixing occurs, is too thin in the climate model, which significantly hinders the model from reproducing the observed evolution of large El Niño events.

Key Points:

- Coupled processes and subsurface dynamics near the eastern edge of the western Pacific (WP) Warm Pool are important for air-sea interactions
- The CESM2 has warm and fresh surface biases in the tropical Pacific Ocean, a too thin barrier layer bias in WP
- Barrier layer thickness biases in the west Pacific and isothermal layer depth biases in east influence the development of El Niño

Correspondence to:
H.-H. Wei,
hohsuan.wei@colorado.edu

Citation:
Wei, H.-H., Subramanian, A. C., Karnauskas, K. B., DeMott, C. A., Mazloff, M. R., & Balmaseda, M. A. (2021). Tropical Pacific air-sea interaction processes and biases in CESM2 and their relation to El Niño development. *Journal of Geophysical Research: Oceans*, *126*, e2020JC016967. https://doi.org/10.1029/2020JC016967

Received 13 NOV 2020
Accepted 1 JUN 2021

1. Introduction

The tropical Pacific Ocean features the warm pool region with sea surface temperatures (SSTs) greater than 28°C in the western Pacific (WP) (e.g., Niiler & Stevenson, 1982). This warm pool is due to the prevailing equatorial trade winds accumulating and homogenizing water to the west. Meanwhile, these winds drive upwelling in the east, giving rise to an eastern Pacific (EP) cold tongue. The resulting thermocline structure is deeper in the west and shallower in the east. Perturbations in the trade winds can yield feedbacks that influence the SST and the whole coupled system (e.g., Bjerknes, 1969), a phenomenon known as El Niño-Southern Oscillation (ENSO).

ENSO is one of the most important climate modes, dominating the climate of tropical Pacific and other regions through teleconnections. Atmosphere-ocean coupling in the Pacific Ocean are important for interannual variations associated with ENSO. Many processes can influence SST, such as prevailing winds and their perturbations, surface fluxes, surface shading by atmospheric convection, freshening by rainfall, upper ocean stabilization, and thermocline adjustments. Within these processes, many observational and modeling studies have demonstrated the link between ENSO dynamics and the variability of the westerly wind burst (WWB), eastern edge of the warm pool, barrier layer, and SST (e.g., Drushka et al., 2015; Gasparin & Roemmich, 2016; Kapur & Zhang, 2012; Lopez et al., 2013; Picaut et al., 1996; Puy et al., 2016; Seiki & Takayabu, 2007). Since the WP warm pool and the corresponding strong convection in this region is one of the key features that stimulate El Niño teleconnections, the shift of the edge of the warm pool plays an important role in the climate systems. The edge of the warm pool, where the warm and fresh water in the west meets the cold and salty water in the east, gives rise to a sharp surface salinity front where salty waters subduct to form the WP barrier layer (e.g., Brown et al., 2015).

The barrier layer, which plays an important role in air-sea interactions, is the layer between the bottom of mixed layer and isothermal layer (i.e., isothermal layer depth [ILD] minus mixed layer depth [MLD]). The formation of the barrier layer could be due to the subduction of salty water, the fresh water coming from the river runoff or precipitation near the surface, fresh water advection, or tilting of vertical salinity fronts (e.g., Cronin & McPhaden, 2002; Sprintall & Tomczak, 1992). The ocean mixed layer is regulated by the density profile, which is itself set by both temperature and salinity. If the isothermal layer is deeper than the isohaline layer, the MLD will be shallower than the isothermal layer, corresponding to the presence of a barrier layer. This kind of vertical profile structure hinders entrainment of cold water from below the MLD, since the water is warm in the barrier layer directly below the MLD. Thus the thickness of the barrier layer leads to differences in the surface temperature response to the same mixing processes. Previous studies have shown that the removal of barrier layer effects (i.e., by modification to the vertical ocean mixing scheme) influences the response of SST and can interfere with El Niño development (e.g., Maes et al., 2002, 2005). In addition, warm water advection may also shift the edge of warm pool and therefore affect ENSO dynamics (e.g., Drushka et al., 2015; Picaut et al., 1996).

The east-west tilt of the ILD at the equator is also one of the key features closely related to ENSO dynamics. The shallow background ILD in the EP, for example, could lead to the warming of SST in the EP through thermocline suppression by the Kelvin waves triggered by WWBs in the WP (e.g., Marshall et al., 2009; Zhang, 2001). These previous results suggest that understanding both the surface and subsurface biases in the tropical Pacific is important for interpreting the climate system, especially in regards to El Niño development and maintenance.

The Community Earth System Model Version 2 (CESM2) is the latest version of the fully coupled, community, global climate model developed by National Center for Atmospheric Research (NCAR). This model and its predecessors are widely used and also contribute to the various phases of the Coupled Model Intercomparison Project (CMIP). Proving to be among the more realistic CMIP models, the CESM2 and its recent predecessors have been shown to capture the ENSO characteristics (e.g., Danabasoglu et al., 2020; Deser et al., 2012). Compared to its previous major release (i.e., CESM1), CESM2 shows substantial improvement (Danabasoglu et al., 2020). For example, CESM2 shows the reductions in low-latitude precipitation and shortwave cloud forcing biases and has better representation of the Madden-Julian Oscillation and ENSO-related teleconnections. However, biases in the CESM2 still exist and need further investigation. Understanding the possible reasons for the biases, and how they relate to the biases of other fields, can help us improve future models and strategies for collecting observational data. In this study, we describe mean state biases in CESM2 and diagnose their implications for the El Niño development.

In this study, we identify climatological biases relevant to air-sea interactions over the tropical Pacific region in the CESM2, and describe the potential relationships between them in the context of a fully coupled system. We further aim to determine how the model biases related to ENSO dynamics may influence the development of El Niño in the model. The data and methodology are described in Section 2. Both the details of the CESM2 model and the reanalysis data used for identifying model biases are introduced. Additionally, the definition of the barrier layer thickness and the associated isothermal and MLDs are described. In Section 3, we present the mean tropical Pacific Ocean state biases of the CESM2 at both the surface and

subsurface. The relationship of the biases with El Niño development is discussed in Section 4. The final section summarizes the discussions and results of this paper.

2. Data and Methodology

2.1. Data Description

We want to advance our understanding of the air-sea interaction processes and their role in ENSO, and also identify possible processes in need of improvement or regions where better observations are needed to constrain models. Hence, we identify the biases in these processes in one of the ensemble members of the CESM2 historical run (Danabasoglu et al., 2020) from the Coupled Model Intercomparison Project 6 (CMIP6). The CESM2 model has coupled atmosphere, land, ocean, sea ice, and ice sheets. The atmospheric component of the CESM2 is Community Atmosphere Model version 6 with 0.9° latitude × 1.25° longitude and 32 levels, while the oceanic component is Parallel Ocean Program version 2 with approximately 1° horizontal resolution with enhanced resolution (around 0.25° in latitude) near the equator (cf. gx1v7 grid resolution) and 60 z-grid vertical levels (uniform 10 m resolution in the upper 160 m, and 250 m resolution from 3,500 m to a maximum depth of 5,500 m with monotonically increasing resolution between 160 and 3,500 m). The historical run is forced by the historical radiative forcing and the model does not assimilate observational data during the model simulation.

To identify the CESM2 biases, we compare the model output with ocean reanalysis from the Ocean ReAnalysis System 5 (ORAS5, Zuo et al., 2019) and atmospheric reanalysis from the ERA-Interim (Dee et al., 2011) from European Center for Medium-Range Weather Forecasts (ECMWF), which are considered to be close to the observational ground-truth. This is because the differences between the model and reanalysis data are mainly caused by the model biases with little influence of climate scenarios and internal variability. The ERA-Interim is used here because it provides the atmospheric state inputs to the ORAS5 over the time period of CESM2 data we analyze. Although the difference between the atmospheric states of the CESM2 and the ERA-Interim could play a role in the biases of the oceanic states, the ORAS5, forced with atmospheric reanalyzes data (i.e., the observational ground-truth of the atmosphere), can be useful for highlighting biases with respect to the true ocean with its high temporal and spatial resolutions.

When assessing the mean state biases, we analyze the same time period of the reanalysis data as the CESM2 output from 1980 to 2014. However, the data of 2015 and 2016 in the ORAS5 are also used for analyzing the 2015–2016 El Niño event. The horizontal resolution of the ORAS5 is 0.25° × 0.25° with 75 z-grid vertical levels (layer center depth from approximately 0.5 to 5,900 m). The spatial resolution of the ERA-Interim is approximately 80 km (T255 spectral) with 60 vertical levels from the surface up to 0.1 hPa.

To compare the model and reanalysis data with different resolutions, we interpolate the horizontal resolution of the two data sets to 1° × 1°. The vertical coordinate of the ORAS5 is interpolated to the vertical coordinate of the CESM2. The surface level in the ocean is therefore centered at 5-m depth (Figure 1).

2.2. Barrier Layer Calculation

Following Sprintall and Tomczak (1992) and Cronin and McPhaden (2002), we define the ILD as the depth where the potential temperature, θ, is $\Delta\theta$ lower than the surface reference level (θ_s). In other words, ILD $= z(\theta = \theta_s - \Delta\theta)$. In our calculation, we select the surface reference depth to be 5 m (i.e., the center depth of the nearest surface level for CESM2 data) and the $\Delta\theta$ as 0.2 K (e.g., Katsura et al., 2015; Mignot et al., 2007; Montégut et al., 2007). The MLD, on the other hand, is the depth where the potential density, σ, is $\Delta\sigma$ higher than the potential density at the surface reference level (σ_s). This means MLD $= z(\sigma = \sigma_s + \Delta\sigma)$, where $\Delta\sigma$ is selected to be the magnitude of a local potential density change equivalent to an 0.2 K potential temperature change (i.e., $\Delta\sigma = \frac{\partial\sigma}{\partial\theta}\Delta\theta$). The barrier layer thickness (BLT) is then the ILD minus the MLD.

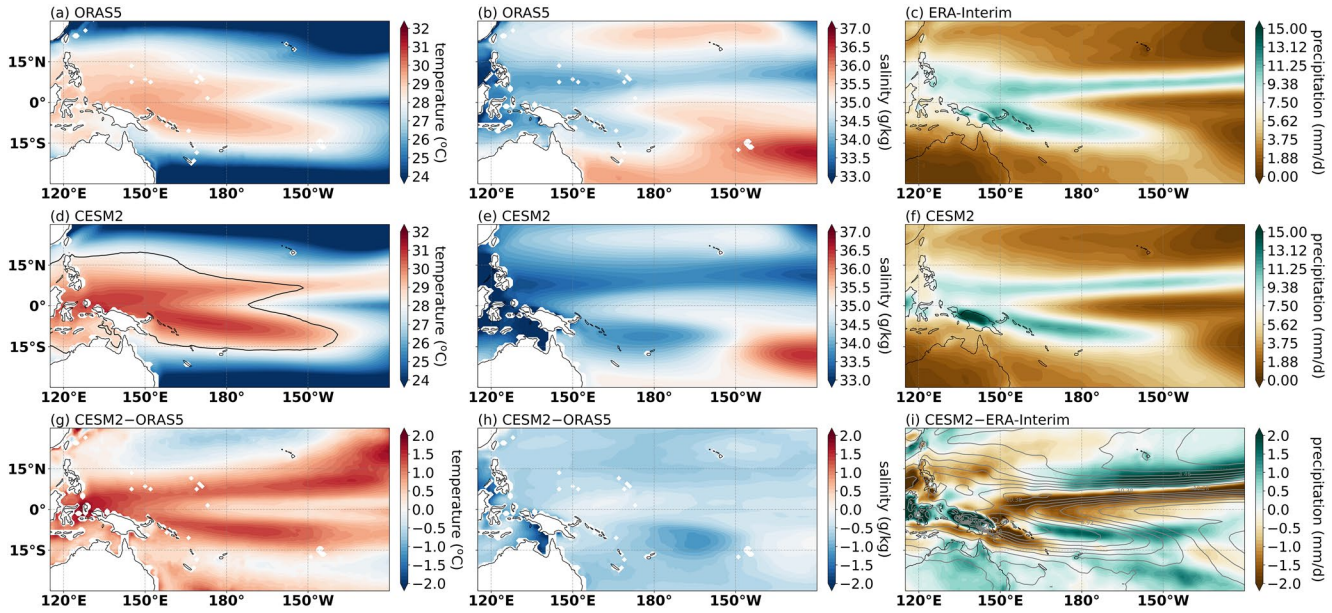

Figure 1. The sea surface temperature (°C) over tropical Pacific Ocean averaged from 1980 to 2014 in (a) Ocean ReAnalysis System 5 (ORAS5), (d) Community Earth System Model version 2 (CESM2), and (g) the biases of CESM2 (CESM2−ORAS5). The white shading corresponds to 28°C isotherm in (a) ORAS5 and (d) CESM2. The black contour in (d) indicates the 28°C isotherm in ORAS5. (b, e, h) Same as (a, d, g) except for the sea surface salinity (g kg^{-1}). (c, f, i) The precipitation (mm d^{-1}) averaged from 1980 to 2014 in (c) ERA-Interim, (f) CESM2, and (i) the biases of CESM2 (CESM2−ERA-Interim). The sea surface temperature and sea surface salinity are the results at 5-m depth, which is the surface level of the CESM2.

3. Mean State Biases

The mean state biases are calculated by averaging for 35 years from 1980 to 2014. The biases of SST and sea surface salinity (SSS) are shown in Figures 1a, 1b, 1d, 1e, 1g, and 1h. In the Pacific deep tropics, the CESM2 has warm surface biases with peaks on both sides of the equator.

The surface salinity in both CESM2 and reanalysis data generally follow the pattern of the precipitation, with fresher water under regions of heavier precipitation (Figures 1b, 1c, 1e, and 1f). Over the equator, ORAS5 and CESM2 both have warmer and fresher water in the west and colder and saltier water in the east. The CESM2, however, is too fresh over the whole tropical Pacific region (Figure 1h) compared to the reanalysis data with a pattern related to the bias in precipitation (Figure 1i). In other words, the relatively smaller fresh biases are found near the equator, which are near the area of dry precipitation bias while the relatively larger fresh biases are near 10°–15°N and °S (by up to −1.2 g kg^{-1}), which are closer to the area of wet precipitation biases. In the CESM2, the Intertropical Convergence Zone (ITCZ) in the Northern Hemisphere (NH) tends to move northward and the Southern Pacific Convergence Zone (SPCZ) is too strong compared to the ERA-Interim reanalysis data (Figures 1c, 1f, and 1i). Similar features can be seen when we compare the model with the observational results from Global Precipitation Climatology Project (not shown).

Based on the subsurface overturning circulation over the central to EP (Figure 2), it is shown that the oceanic subtropical overturning cells in the CESM2 have weak biases. This bias in velocity corresponds to a weaker cold advection away from the equator near the surface due to the potential temperature structure in the ocean and weaker upwelling of cold water at the equator, which may result in the warmer biases at the two sides of the equator shown in Figure 1g. High precipitation biases have been shown to be associated with warm SST biases (e.g., Xie et al., 2010), which is consistent to the wet biases over the region with warm SST biases in CESM2 (Figures 1g and 1i). While the surface salinity in the CESM2 is in general too fresh over the whole tropical Pacific region, the higher fresh biases are generally located near the central Pacific away from the equator, where the precipitation also has higher wet biases (Figures 1h and 1i). This suggests that the weak biases in subtropical cell strength could be one of the reasons of the warm SST biases and therefore the pattern of precipitation and salinity biases. While the subtropical cell strength in the CESM2 is weaker than the ORAS5, the CESM2 easterly wind stress is not weaker (not shown). This suggests that the weak

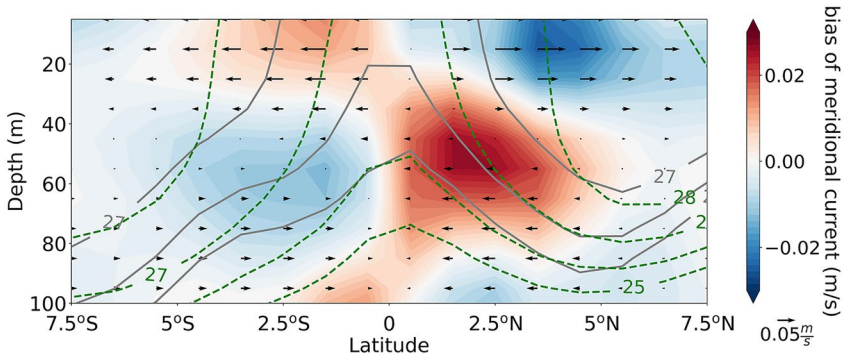

Figure 2. Zonal mean meridional current (vector, unit: m/s) and potential temperature (gray contour, unit: °C with 1°C interval) in the Ocean ReAnalysis System 5 (ORAS5) averaged between 180° and 110°W. Zonal mean potential temperature in Community Earth System Model version 2 (CESM2) (green dashed contour, unit: °C with 1°C interval). The shading shows the biases of meridional current of the CESM2 (CESM2−ORAS5). Here, only contours larger than 25°C are shown.

biases of subtropical cells are likely not due to the weak biases of surface wind stress. They might be related to the biases of other processes (e.g., the geostrophic flow and the internal mixing processes which can lead to biases in the momentum transport and distribution of the density).

For the subsurface ocean features, while the large-scale vertical structure of temperature and salinity at the equator is well-captured by the CESM2, there is strong warm bias near the thermocline in the EP corresponding to a deep bias of ILD (Figures 3a, 3c, and 3e). Meanwhile, the fresh biases spread throughout the equatorial Pacific upper ocean. The stronger fresh biases near the level of the salinity maximum in the WP favors the deepening of the level of maximum salinity stratification, and corresponds to a deep bias in MLD, which is related to the biases of the level of salinity stratification (Figures 3b, 3d, and 3f).

To quantify the biases of the subsurface ocean structure, we calculate the MLD, ILD, and BLT based on the definition introduced in Section 2b at different longitudes over the equator (Figure 4). The mean vertical profiles of potential temperature, salinity, and potential density at 160°E and 120°W are shown in

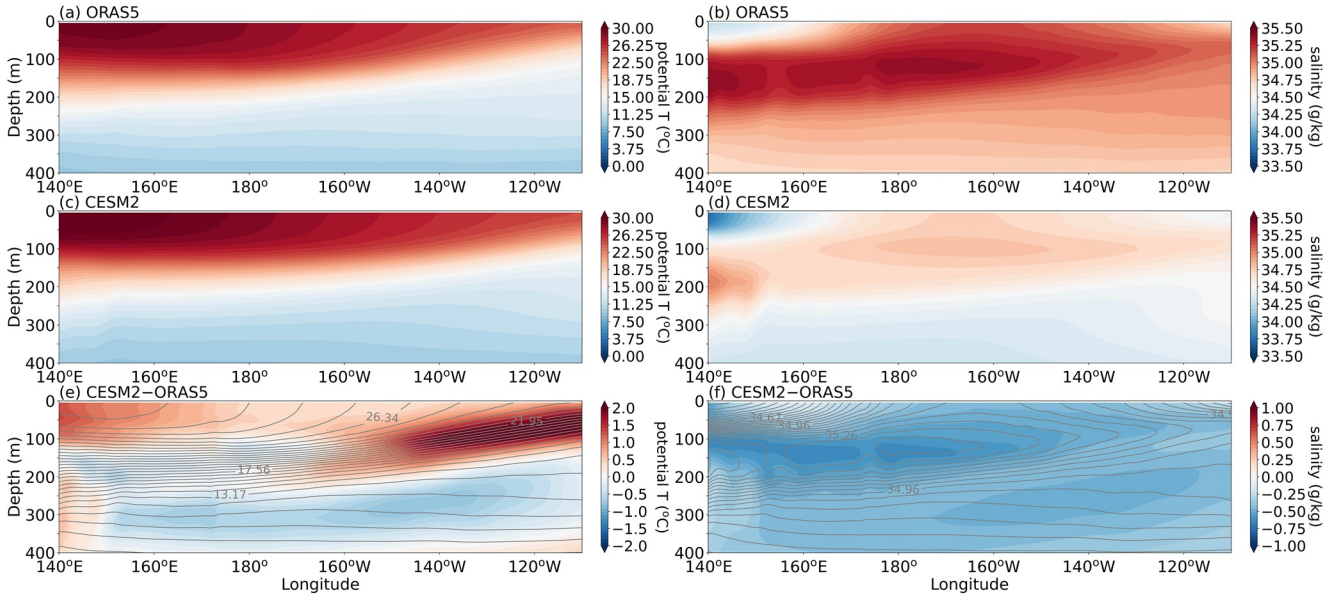

Figure 3. Longitude-depth cross sections of potential temperature (°C) from (a) Ocean ReAnalysis System 5 (ORAS5), (c) Community Earth System Model version 2 (CESM2), and (e) the biases of CESM2, averaged within 2°S to 2°N. (b, d, f) Same as (a, c, e) except for salinity (g kg^{-1}). The contours in (e and f) are potential temperature and salinity in ORAS5 (i.e., shading in (a and b)).

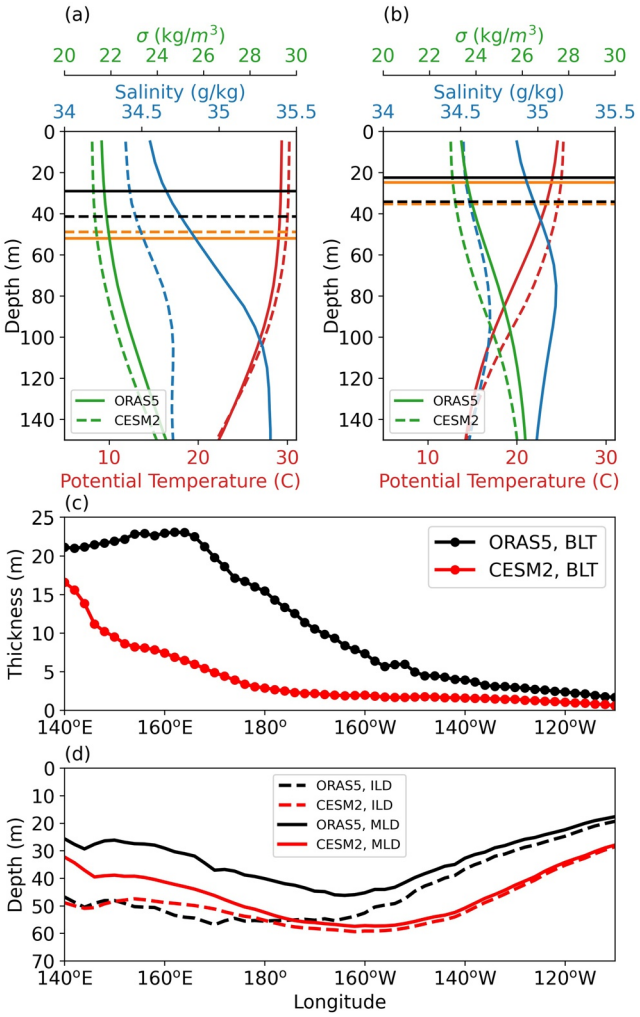

Figure 4. Mean vertical profiles of the potential temperature (red), salinity (blue), and potential density (green) for Ocean ReAnalysis System 5 (ORAS5) (solid) and Community Earth System Model version 2 (CESM2) (dashed) at (a) 160°E and (b) 120°W. The isothermal layer depth (ILD) (mixed layer depth [MLD]) is indicated by the horizontal orange (black) line for ORAS5 (solid) and CESM2 (dashed) from 2°S to 2°N. The longitudinal distribution of the (c) barrier layer thickness (BLT), (d) ILD (dashed) and MLD (solid) for ORAS5 (black) and CESM2 (red).

Figures 4a and 4b, representing the profiles at the western and EP respectively. We can again see the much fresher water in the CESM2 at the level of high salinity in ORAS5 in the WP (blue lines in Figure 4a, near the depth at 140 m) and the deeper warm water in the CESM2 in the EP compared to the ORAS5 (red lines in Figure 4b). The long-term mean BLT is around 20 m in the WP and approaches zero in the EP in the reanalysis data (black dots in Figure 4c). The thick barrier layer in the WP is due to the strong precipitation in the WP combined with convergence of salty water as it is subducted from the east edge of warm pool (e.g., Brown et al., 2015; Sprintall & Tomczak, 1992). The BLT in the CESM2 in the WP is biased thin mainly due to the deep MLD biases (red dots in Figure 4c and solid lines in Figure 4d). In the EP, both the MLD and ILD have deep biases, but the BLT biases are negligible since they are near zero for both model and reanalysis data (Figures 4c and 4d). These deep MLD and ILD biases in the EP are consistent with the weaker subtropical overturning cells we identify in the central to EP, which correspond to a weaker upwelling and deeper thermocline at the equator (e.g., Johnson et al., 2002).

These results suggest that for the mean state biases of the CESM2 model, the precipitation tends to shift away from the equator, which corresponds to warm SST biases with peaks on both sides of the equator. Based on previous studies (e.g., Capotondi et al., 2005; England et al., 2014; Meehl et al., 2013), this may be related to the weak subtropical cells biases in the central and EP, which could influence the SST with weak biases in cold advection on both sides of the equator. The pattern of the fresh SSS bias (fresh biases with peaks on both sides of the equator) is also related to the pattern of precipitation biases and possibly the weak biases of the subtropical cells. The salinity biases could also influence the MLD and BLT biases, which are related to the salinity stratification. Because (a) the tilt of the ILD in the Pacific basin is important for El Niño dynamics and (b) the BLT in the WP has been shown to be important for the development of El Niño (e.g., Maes et al., 2005), these biases of ILD and BLT could play a role in the simulation of El Niño evolution through subsurface vertical processes, which we examine in the following section.

4. Relation With El Niño Development

Air-sea interaction processes and the subsurface ocean structures play important roles in the development of El Niño events. The sensitivity of the atmospheric response to SST changes can also influence the El Niño development (e.g., Yeh et al., 2012). Different mechanisms are capable of influencing the development of warm SST anomalies during El Niño. One of the important processes is the WWB (e.g., Fedorov, 2002; Philander, 1981). While WWB events happen in the WP and propagate toward the central Pacific, there are two pathways that can contribute to warmer SST (Figure 5). First, WWB events can advect warm water from the WP toward the east and reduce surface heat fluxes due to weaker surface trade wind speeds offset by WWBs, which help the local warm SST in the WP expand toward the central Pacific (Figures 5a and 5c). Meanwhile, the WWB events could also trigger eastward-propagating downwelling Kelvin waves by inducing convergence at the equator. Upon reaching the EP, where the background thermocline is shallow, the downwelling Kelvin wave deepens the thermocline, and reduces cooling by upwelling and vertical mixing (Figures 5b and 5d) (e.g., Karnauskas, 2013). These suggest both the local and remote responses of the WWB events are closely related to the El Niño development.

To investigate how subsurface ocean structure biases may influence the development of the El Niño events in the model and reanalysis data respectively, we analyze strong El Niño events in both the model and

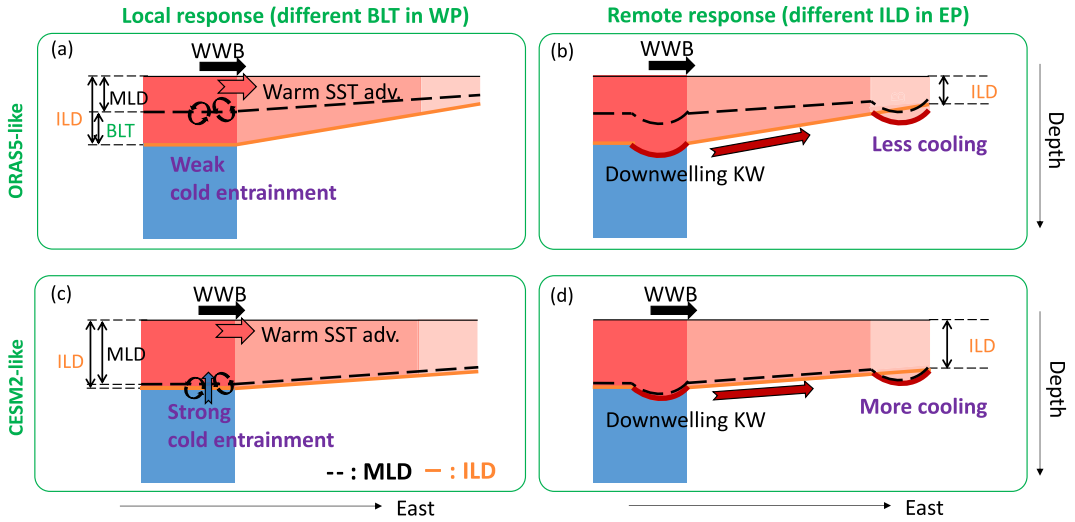

Figure 5. Schematic of the processes triggered by westerly wind bursts (WWBs), which are closely related to the development of El Niño. The upper (lower) figures represent situations more similar to the results in Ocean ReAnalysis System 5 (ORAS5) (Community Earth System Model version 2 [CESM2]). The left (right) figures show the local (remote) response triggered by WWB. The figures are longitude-depth cross section over tropical Pacific basin. The black dashed (orange solid) line indicates the bottom of the mixed layer depth (MLD) (isothermal layer depth [ILD]). The purple texts describe the end states of these processes. Explanation of the schematic: (a and c) The WWB enhances the zonal current and therefore advects warm water eastward. At the same time, with stronger wind stress, it will increase mixing in the ocean. The mixing, trapped in the mixed layer, will induce cold entrainment when the barrier layer thickness (BLT) is too thin (i.e., CESM2-like condition shown in (c)). (b and d) The WWB-triggered downwelling Kelvin waves would propagate eastward and reduce the cooling (i.e., increase sea surface temperature [SST]) in the EP. With a thicker ILD (CESM2-like condition shown in (d)), it will reduce the cooling less (i.e., more cooling). Notice that here we do not specify the possible difference of the zonal advection, which is not the main focus and can be influenced by many different factors including MLD.

reanalysis data, which are defined as Niño 3.4 index larger than 2.5 K. The high Nino3.4 threshold and therefore small sample size (three events for model and reanalysis data respectively during the time period of our data) are used to reduce the variability of the El Niño events we analyze due to different strengths of the events. The moderate and weak El Nino events are not considered in this study since we aim to focus on the events with strong El Niño signals. While these are El Niño events with specific years in the CESM2 (event1: 1993–1994, event2: 2006–2007, event3: 2012–2013) and ORAS5 (event1: 1982–1983, event2: 1997–1998, event3: 2015–2016), the El Niño years of the CESM2 are not expected to correspond to the specific years of the real El Niño events (i.e., the El Niño years of ORAS5) because the El Niño is a variability due to the chaotic nature of the climate system. Therefore, we will use the number of the event when referring to these events for the following discussion (i.e., CESM2 event1, CESM2 event2, CESM2 event3).

The monthly evolution of the SST anomalies of each El Niño event over two calendar years and their composites are shown in Figure 6. In the first half of the first year, a warm SST anomaly develops in the WP and propagates eastward. This is the feature corresponding to the advection of warm waters by the WWB events (Figures 5a and 5c). It is seen in both model and reanalysis data, but is more clear in the reanalysis data. In the second half of the first year, the warm SST anomalies over central and EP develop, likely due to a remote response to the WWB events through Kelvin waves (Figures 5b and 5d), and are likely amplified through the Bjerknes feedback, which is the positive feedback of the zonal SST gradient and zonal surface wind stress (Bjerknes, 1969). Some pattern differences of their evolution are seen between the model and the reanalysis data. In the CESM2, the warm SST anomalies develop and then propagate westward with a break near October of the first composite year (Figures 6e–6g). In the ORAS5, the SST anomalies tend to sustain in the central and EP after the development (Figures 6a–6c). These differences are even clearer in the composites of the three events (Figures 6d and 6h).

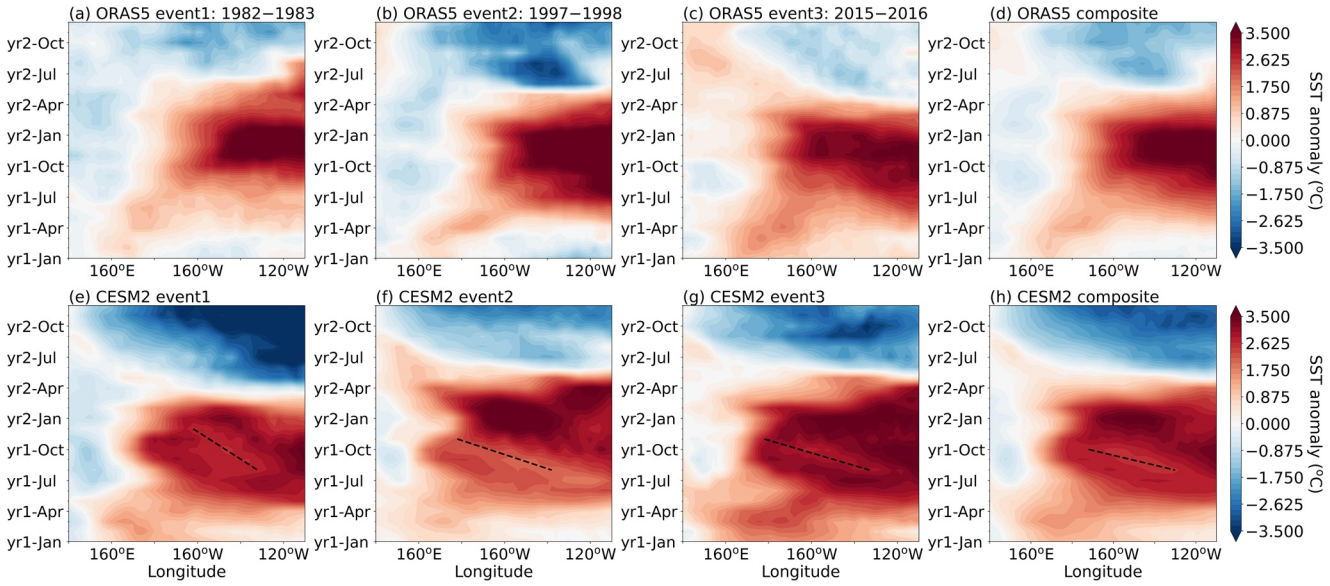

Figure 6. Hovmöller diagram of the equatorial (2°S–2°N) sea surface temperature (SST) anomaly evolution at different longitudes for strong El Niño events in (a–c) Ocean ReAnalysis System 5 (ORAS5) and (e–g) Community Earth System Model version 2 (CESM2). The strong El Niño events are selected based on the Niño3.4 index (averaged SST anomaly within 170°W–120°W and 5°S–5°N). (d and h) The composites of the three events in the ORAS5 and CESM2, respectively. The black dashed lines in (e–h) indicate the break of the warm SST in CESM2.

4.1. Biases of BLT and ILD

Here we explore how model biases in the ocean subsurface structure may contribute to biases in El Niño development. To better relate the processes, the evolution of the BLT and ILD are shown with the evolution of the SST anomalies (Figure 7). It is clear that the BLT is too thin in the CESM2 over the WP before the development of El Niño (Figures 7a, 7c, and 8b contours near the 140°E–160°W and yr1-May to yr1-July). While the WWBs advect the warm water eastward from the western to central Pacific, this thick barrier layer in the ORAS5 could reduce cooling caused by mixing induced by the wind burst (Figure 5a). Meanwhile, the thinner BLT in the CESM2 would have less of a barrier effect, thus causing cooling biases in the WP during the warm SST anomaly expansion eastward by the zonal advection (Figure 5c). The ILD, on the other hand, shows deep biases in the CESM2 in the EP before the development of El Niño (Figures 7b, 7d, and 8d contours near the 110°–150°W and yr1-April to yr1-August). The less tilted thermocline in the CESM2 corresponds to a slightly weaker Bjerknes feedback (Bjerknes, 1969), which may slow the El Niño development and may lead to the failure of the warm SST anomaly moving eastward in the model. While the deep ILD bias itself may potentially influence El Niño development through reducing the Bjerknes feedback, here we focus on the processes responding to the WWB. When the downwelling Kelvin waves reach the EP, suppression of the shallow background ILD is the key feature enhancing the warming of SST in the EP (Figure 5b). The ILD thick biases here, therefore, reduce the warming anomalies due to the relatively lower ratio of the deepening of the ILD, which yields less reduction of upwelling and mixing processes and leads to a cooling bias in the EP (Figure 5d).

To quantify the influence of the biases of BLT and ILD on the mixing and entrainment processes, the anomalous vertical advection and entrainment (VAE) term in the mixed layer heat budget is shown in Figure 8. The mixed layer heat budget describes how the tendency of the mixed layer temperature is influenced by different terms: the horizontal advection term, the surface heat flux forcing term, and the VAE term (e.g., Li et al., 2016; Stevenson & Niiler, 1983). The anomalies of these terms can drive the anomaly of the mixed layer temperature tendency, which characterizes the El Niño development. While all of these anomalous terms can influence the evolution of the mixed layer temperature anomaly, here, we focus on the impact of the anomalous VAE term, which is the term capturing the influence of the processes we focus on due to the WWB events (i.e., the cold entrainment due to mixing in the WP and the reduction of cooling (i.e., warming) due to downwelling Kelvin waves reaching the EP). The biases of the anomalous VAE term is therefore

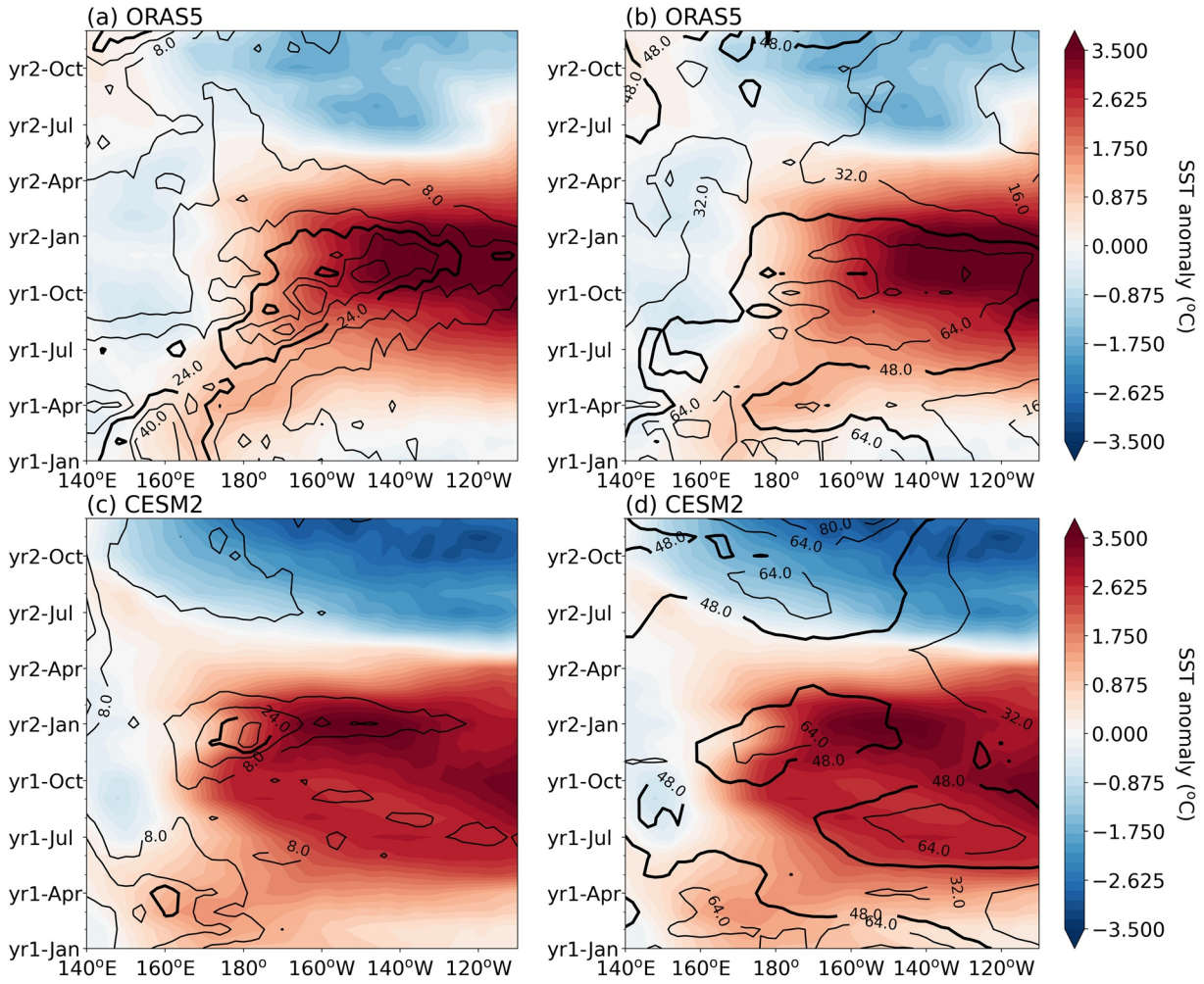

Figure 7. The contour shows the barrier layer thickness (m) evolution for the composite of El Niño events in (a) Ocean ReAnalysis System 5 (ORAS5) and (c) Community Earth System Model version 2 (CESM2). (b and d) Same as the contour in (a and c) except for isothermal layer depth (m). The shading in (a and b) are the same as Figure 6d and the shading in (c and d) are the same as Figure 6h.

the term that can be changed by the biases of BLT and ILD. The VAE term is calculated as $-w_e \frac{\Delta\theta}{\mathrm{MLD}}$, where the entrainment velocity w_e is defined as $w_{MLD} + \frac{d\mathrm{MLD}}{dt}$, w_{MLD} is the vertical velocity at the level of MLD (i.e., $\frac{dz}{dt}|_{z=MLD}$), and Δ is the difference between the value within mixed layer (10 m above MLD) and the value 10 m below mixed layer (e.g., Li et al., 2016; Stevenson & Niiler, 1983). It is clear that in the EP before the peak of the El Niño events, the CESM2 has much weaker warming, which is consistent with the deeper background ILD bias (around yr1-April to yr1-August and 150°W–110°W in Figure 8d). In the WP before the peak of the El Niño events (around yr1-May to yr1-September and 140°E–160°W, see region highlighted by yellow ellipse in Figure 8b), the heating term through the VAE is smaller in the CESM2 (i.e., cooling biases); this cooling bias follows the too-thin BLT bias (contours), suggesting that when the CESM2 BLT bias is sufficiently thin, it would increase the cooling by vertical processes. Near the mature phase of El Niño (around yr1-December), the VAE term is also much smaller in the CESM2. This suggests the thin biases of BLT during El Niño in the CESM2 favors cooling from vertical mixing, which interferes with the development of warm SST anomalies and hinders the maintenance of the warm SST during El Niño.

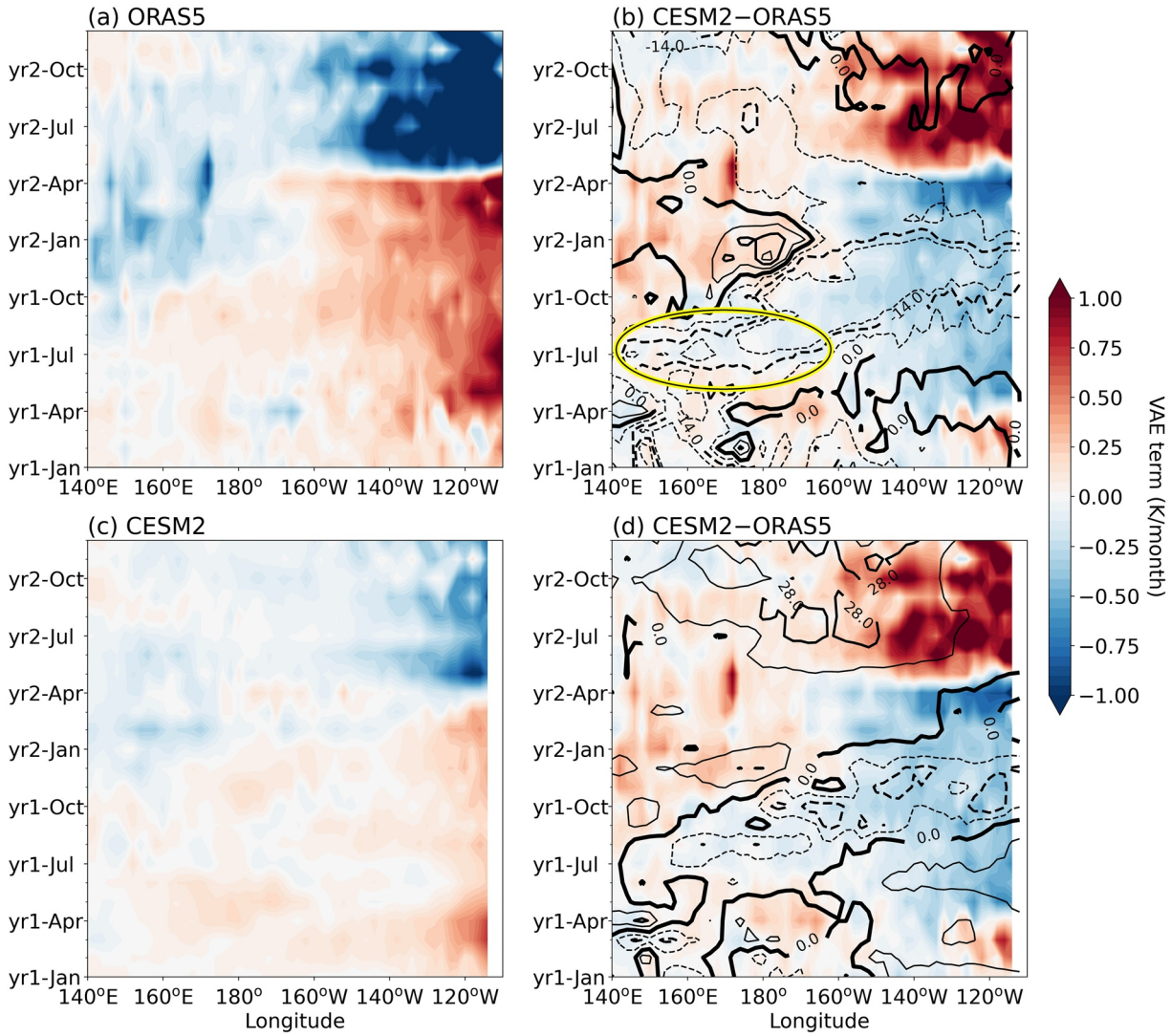

Figure 8. Evolution of the anomalous vertical advection and entrainment (VAE) term $-w_e \frac{\Delta\theta}{\mathrm{MLD}}$ (K month^{-1}) for (a) Ocean ReAnalysis System 5 (ORAS5), (c) Community Earth System Model version 2 (CESM2), and (b and d) the biases (CESM2−ORAS5, shading). The contours are the biases of (b) barrier layer thickness (m, the contour interval is 7 m) and (d) isothermal layer depth (m, the contour interval is 14 m). The thickest solid contours are 0 m and the second thickest solid/dashed contours are (b) ±14 m and (d) ±28 m. The yellow ellipse in (b) highlights the concurrence of a negative difference in the anomalous VAE term and a thin BLT bias.

4.2. Biases of Sea Surface Temperature Annual Cycle

In Figure 6, we can clearly see that the difference in the evolution of the El Niño for CESM2 and ORAS5 includes a westward-propagating break of warm SST anomalies in the CESM2 near the fall of the first composite year, while the warm SST anomalies are sustained much more consistently in the ORAS5. From the composites of the total SST (i.e., the sum of the monthly climatology and the SST anomaly) evolution for the strong El Niño events (Figures 9a and 9d), the warm total SST over the central Pacific tends to propagate eastward with time in the ORAS5, while in the CESM2, the warm total SST tends to have a clearer westward retreat near boreal fall of the first composite year (east of 180°). This leads us to hypothesize that the break corresponds to biases in the seasonal cycle signal in the central to EP in the CESM2, which has a monthly SST climatology biased cold in the EP and CP around boreal fall at the equator (Figures 9b, 9e, and 9c). The cold signal of the SST annual cycle from August to November is stronger in the CESM2 and extends from the EP toward the central Pacific (shown in Figures 9c and 9f), and this may act to interrupt

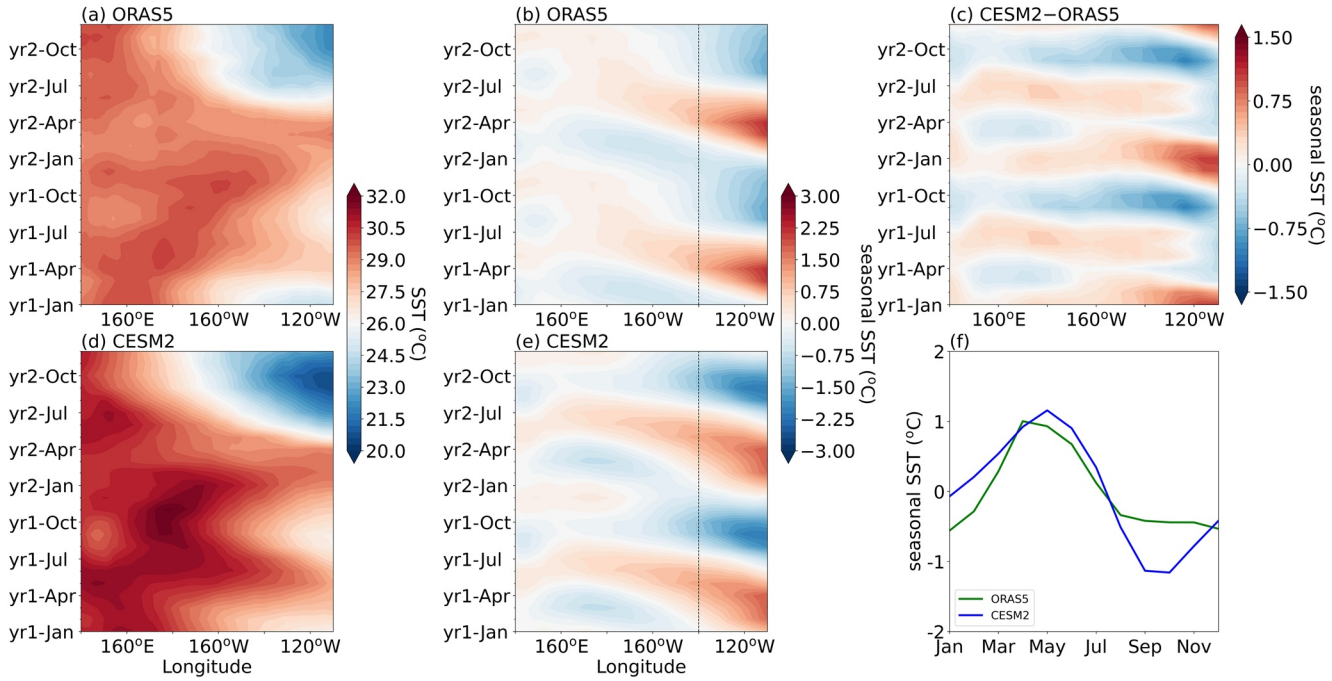

Figure 9. Evolution of the total sea surface temperature (SST) in the (a) Ocean ReAnalysis System 5 (ORAS5) and (d) Community Earth System Model version 2 (CESM2) for the strong El Niño composite. The evolution of the SST seasonal signal, in which the annual mean total SST at each longitude is subtracted from the monthly climatology SST, in the (b) ORAS5 and (e) CESM2. (c) The biases of the evolution of the SST seasonal signal (i.e., (e) minus (b)). (f) The SST seasonal signal at the 140°W in ORAS5 (green, corresponding to the SST seasonal signal indicated by the dashed line in (b)) and CESM2 (blue, corresponding to the dashed line in (e)).

the development of the warm SST anomalies during the El Niño events. It is likely that the mechanisms behind the biases in the background SST annual cycle are also contributing to the difference of the El Niño development between the reanalysis data and CESM2.

5. Discussion and Conclusion

In this study, the mean state biases of the surface and subsurface tropical Pacific Ocean in the CESM2 are identified and the relation of these biases to El Niño development are discussed in the context of local processes as well as basin scale dynamics. It is shown that there are warm surface biases in the Pacific deep tropics with peaks on both sides of the equator. The ITCZ in the NH shifts northward and the SPCZ is too strong in the CESM2. The fresh surface salinity biases are found across the tropical Pacific region with higher biases at the regions with wet precipitation biases. As for the subsurface ocean features, strong warm biases are located at the thermocline depth in the EP, which corresponds to deep ILD and MLD biases. The biases of the salinity peaks at the levels with high subsurface salinity values in the WP, which corresponds to a deep MLD bias and therefore a thin BLT bias.

The biases in SST, precipitation, ILD, and MLD are likely related to the biases in subtropical overturning cell in the central and EP because the weak meridional circulation biases lead to weaker cold surface advection away from the equator, resulting in the warm SST biases and corresponding biases in precipitation and salinity. The weaker meridional circulation biases would also correspond to weak upwelling biases at the equator, which is related to deep ILD and MLD biases in the EP.

The relationship between the surface and subsurface biases and El Niño development are examined. During strong El Niño events, the SST anomaly pattern evolves differently for CESM2 and ORAS5. While they both exhibit propagation of warm SST anomalies from the western to central Pacific in the early months of the first composite year and the emergence of warm anomalies through Kelvin waves in the central and EP later, in the CESM2, the developed SST anomaly in the EP tends to migrate

westward with a break of warm SST near the October of the first composite year. In the ORAS5, on the other hand, the SST anomaly developed in the CP and EP tends to persist throughout the El Niño evolution. Before the onset of El Niño, the corresponding evolution of the BLT shows thin biases in the WP and the ILD shows deep biases in the EP. The thin BLT biases in the WP and the corresponding reduced barrier effect of the barrier layer correspond to cooling biases due to the VAE, which is shown in the analysis of the mixed layer heat budget. Notice that these BLT biases need to be large enough in order to see response in the heat budget since a thinner but thick enough BLT could still lead to barrier effects. As for the deep ILD biases in the EP, they reduce the SST warming associated with the downwelling Kelvin waves reaching the EP with shallow background ILD, as reflected in the VAE term in the mixed layer heat budget with cooling biases in the CESM2. This is because the ratio of the perturbed and background ILD due to the downwelling Kelvin waves is smaller if the background ILD is deeper. The relationships between these mean subsurface ocean biases and ENSO processes are summarized in Figure 5.

Here, while we analyze the VAE term to identify the influence of the BLT on the mixed layer temperature anomaly tendency, the VAE term can also be influenced by the strength of the wind stress anomaly, the vertical gradient of the temperature across the thermocline, and the depth of the mixed layer. Due to the nonlinearity of the influences from these features, it is hard to isolate the individual impact. In this paper, we only focus on the influence of the BLT and show a relationship between the BLT and the mixed layer temperature tendency through VAE term.

Other than the subsurface ocean features, we also show that the CESM2 has strong SST biases in the equatorial seasonal cycle, especially with strong cold biases in the boreal fall. The strong cold biases of the monthly climatological seasonal cycle, which is especially clear in the central and EP, could interfere with the development of warm SST anomalies, which can be related to the break of the warm SST anomaly in the CESM2 near October of the first composite year.

While we discuss how some of the biases influence El Niño development through specific processes that are influenced by WWBs, there are many other pathways that can play important roles in ENSO events. For example, the extratropical climate variability could influence different patterns of El Niño development (e.g., Yu et al., 2015). The difference in the frequency and strength of WWB events could also lead to different development of El Niño events. The other terms in the surface heat budget (e.g., the horizontal advection and surface forcing) could also be different due to the biases of the background states and anomalies.

While we only looked at the results in the CESM2, it will be beneficial to explore whether other models also provide similar insights on equatorial ocean circulation biases and their relationship to the biases of the subsurface ocean structure as well as the annual cycle of SST and the El Niño development. For example, the subtropical cells may be sensitive to the wide range of physical processes and parameterizations including horizontal diffusion (Maes et al., 1997), eddies (Brown et al., 2007), entrainment (Pedlosky, 1988) and vertical mixing (Yu & Schopf, 1997), and barrier layer thickness may be sensitive to freshwater fluxes and upper ocean mixing. These biases and their influences on the climate system could provide information for future observations, such as the Tropical Pacific Observing System 2020 (TPOS2020) process studies, which could further help improve observation of the above mentioned physical processes, and therefore the model representation of these processes.

Data Availability Statement

All data are publicly available and/or drawn from primary sources cited in the main text. The ERA-Interim data were downloaded from ECMWF website https://www.ecmwf.int/en/forecasts/datasets/reanalysis-datasets/era-interim, the ORAS5 data were downloaded from Integrated Climate Data Center https://icdc.cen.uni-hamburg.de/daten/reanalysis-ocean/easy-init-ocean/ecmwf-oras5.html, and the CESM2 output we analyzed are the output of CMIP6, which can be downloaded from CMIP6 website https://esgf-node.llnl.gov/search/cmip6/ or NCAR GLADE collections.

Acknowledgments
This work was supported by the NOAA grant (NA18OAR4310405 and NA18OAR4310406) and the CIRES visiting fellowship. The analyses were conducted on the CU Boulder Indopac computing cluster and NCAR Cheyenne cluster.

References

Bjerknes, J. (1969). Atmospheric teleconnections from the equatorial Pacific. *Monthly Weather Review*, *97*(3), 163–172. https://doi.org/10.1175/1520-0493(1969)097<0163:atftep>2.3.co;2

Brown, J. N., Godfrey, J. S., & Fiedler, R. (2007). A zonal momentum balance on density layers for the central and eastern equatorial pacific. *Journal of Physical Oceanography*, *37*(7), 1939–1955. https://doi.org/10.1175/jpo3090.1

Brown, J. N., Langlais, C., & Sen Gupta, A. (2015). Projected sea surface temperature changes in the equatorial Pacific relative to the Warm Pool edge. *Deep Sea Research Part II: Topical Studies in Oceanography*, *113*, 47–58. https://doi.org/10.1016/j.dsr2.2014.10.022

Capotondi, A., Alexander, M. A., Deser, C., & McPhaden, M. J. (2005). Anatomy and decadal evolution of the Pacific subtropical–tropical cells (STCs). *Journal of Climate*, *18*(18), 3739–3758. https://doi.org/10.1175/JCLI3496.1

Cronin, M. F., & McPhaden, M. J. (2002). Barrier layer formation during westerly wind bursts. *Journal of Geophysical Research*, *107*(C12). https://doi.org/10.1029/2001JC001171

Danabasoglu, G., Lamarque, J.-F., Bacmeister, J., Bailey, D. A., DuVivier, A. K., Edwards, J., et al. (2020). The Community Earth System Model Version 2 (CESM2). *Journal of Advances in Modeling Earth Systems*, *12*(2), e2019MS001916. https://doi.org/10.1029/2019MS001916

Dee, D. P., Uppala, S. M., Simmons, A. J., Berrisford, P., Poli, P., Kobayashi, S., et al. (2011). The ERA-Interim reanalysis: Configuration and performance of the data assimilation system. *Quarterly Journal of the Royal Meteorological Society*, *137*(656), 553–597. https://doi.org/10.1002/qj.828

Deser, C., Phillips, A. S., Tomas, R. A., Okumura, Y. M., Alexander, M. A., Capotondi, A., et al. (2012). ENSO and Pacific decadal variability in the community climate system model version 4. *Journal of Climate*, *25*(8), 2622–2651. https://doi.org/10.1175/JCLI-D-11-00301.1

Drushka, K., Bellenger, H., Guilyardi, E., Lengaigne, M., Vialard, J., & Madec, G. (2015). Processes driving intraseasonal displacements of the eastern edge of the warm pool: The contribution of westerly wind events. *Climate Dynamics*, *44*(3), 735–755. https://doi.org/10.1007/s00382-014-2297-z

England, M. H., McGregor, S., Spence, P., Meehl, G. A., Timmermann, A., Cai, W., et al. (2014). Recent intensification of wind-driven circulation in the Pacific and the ongoing warming hiatus. *Nature Climate Change*, *4*(3), 222–227. https://doi.org/10.1038/nclimate2106

Fedorov, A. V. (2002). The response of the coupled tropical ocean–atmosphere to westerly wind bursts. *Quarterly Journal of the Royal Meteorological Society*, *128*(579), 1–23. https://doi.org/10.1002/qj.200212857901

Gasparin, F., & Roemmich, D. (2016). The strong freshwater anomaly during the onset of the 2015/2016 El Niño. *Geophysical Research Letters*, *43*, 6452–6460. https://doi.org/10.1002/2016GL069542

Johnson, G. C., Sloyan, B. M., Kessler, W. S., & McTaggart, K. E. (2002). Direct measurements of upper ocean currents and water properties across the tropical Pacific during the 1990s. *Progress in Oceanography*, *52*(1), 31–61. https://doi.org/10.1016/S0079-6611(02)00021-6

Kapur, A., & Zhang, C. (2012). Multiplicative MJO forcing of ENSO. *Journal of Climate*, *25*(23), 8132–8147. https://doi.org/10.1175/JCLI-D-11-00609.1

Karnauskas, K. B. (2013). Can we distinguish canonical El Niño from Modoki? *Geophysical Research Letters*, *40*, 5246–5251. https://doi.org/10.1002/grl.51007

Katsura, S., Oka, E., & Sato, K. (2015). Formation mechanism of barrier layer in the subtropical Pacific. *Journal of Physical Oceanography*, *45*(11), 2790–2805. https://doi.org/10.1175/JPO-D-15-0028.1

Li, Y., Han, W., Wang, W., & Ravichandran, M. (2016). Intraseasonal variability of SST and precipitation in the Arabian Sea during the Indian Summer Monsoon: Impact of ocean mixed layer depth. *Journal of Climate*, *29*(21), 7889–7910. https://doi.org/10.1175/JCLI-D-16-0238.1

Lopez, H., Kirtman, B. P., Tziperman, E., & Gebbie, G. (2013). Impact of interactive westerly wind bursts on CCSM3. *Dynamics of Atmospheres and Oceans*, *59*, 24–51. https://doi.org/10.1016/j.dynatmoce.2012.11.001

Maes, C., Madec, G., & Delecluse, P. (1997). Sensitivity of an equatorial Pacific OGCM to the lateral diffusion. *Monthly Weather Review*, *125*(5), 958–971. https://doi.org/10.1175/1520-0493(1997)125<0958:soaepo>2.0.co;2

Maes, C., Picaut, J., & Belamari, S. (2002). Salinity barrier layer and onset of El Niño in a Pacific coupled model. *Geophysical Research Letters*, *29*(24). https://doi.org/10.1029/2002GL016029

Maes, C., Picaut, J., & Belamari, S. (2005). Importance of the salinity barrier layer for the buildup of El Niño. *Journal of Climate*, *18*(1), 104–118. https://doi.org/10.1175/JCLI-3214.1

Marshall, A. G., Alves, O., & Hendon, H. H. (2009). A coupled GCM analysis of MJO activity at the onset of El Niño. *Journal of the Atmospheric Sciences*, *66*(4), 966–983. https://doi.org/10.1175/2008JAS2855.1

Meehl, G. A., Hu, A., Arblaster, J. M., Fasullo, J., & Trenberth, K. E. (2013). Externally forced and internally generated decadal climate variability associated with the interdecadal Pacific oscillation. *Journal of Climate*, *26*(18), 7298–7310. https://doi.org/10.1175/JCLI-D-12-00548.1

Mignot, J., Montégut, C. d. B., Lazar, A., & Cravatte, S. (2007). Control of salinity on the mixed layer depth in the world ocean: 2. Tropical areas. *Journal of Geophysical Research*, *112*, C06011. https://doi.org/10.1029/2006JC003954

Montégut, C. d. B., Mignot, J., Lazar, A., & Cravatte, S. (2007). Control of salinity on the mixed layer depth in the world ocean: 1. General description. *Journal of Geophysical Research*, *112*(C6), C06011. https://doi.org/10.1029/2006JC003953

Niiler, P., & Stevenson, J. (1982). The heat budget of tropical ocean warm-water pools. *Journal of Marine Research*, *17*.

Pedlosky, J. (1988). Entrainment and the termination of the equatorial undercurrent. *Journal of Physical Oceanography*, *18*(6), 880–886. https://doi.org/10.1175/1520-0485(1988)018<0880:eattot>2.0.co;2

Philander, S. G. H. (1981). The response of equatorial oceans to a relaxation of the trade winds. *Journal of Physical Oceanography*, *11*(2), 176–189. https://doi.org/10.1175/1520-0485(1981)011<0176:TROEOT>2.0.CO;2

Picaut, J., Ioualalen, M., Menkes, C., Delcroix, T., & McPhaden, M. J. (1996). Mechanism of the zonal displacements of the Pacific warm pool: Implications for ENSO. *Science*, *274*(5292), 1486–1489. https://doi.org/10.1126/science.274.5292.1486

Puy, M., Vialard, J., Lengaigne, M., & Guilyardi, E. (2016). Modulation of equatorial Pacific westerly/easterly wind events by the Madden–Julian oscillation and convectively-coupled Rossby waves. *Climate Dynamics*, *46*(7–8), 2155–2178. https://doi.org/10.1007/s00382-015-2695-x

Seiki, A., & Takayabu, Y. N. (2007). Westerly wind bursts and their relationship with intraseasonal variations and ENSO. Part I: Statistics. *Monthly Weather Review*, *135*(10), 3325–3345. https://doi.org/10.1175/MWR3477.1

Sprintall, J., & Tomczak, M. (1992). Evidence of the barrier layer in the surface layer of the tropics. *Journal of Geophysical Research*, *97*(C5), 7305. https://doi.org/10.1029/92JC00407

Stevenson, J. W., & Niiler, P. P. (1983). Upper ocean heat budget during the Hawaii-to-Tahiti shuttle experiment. *Journal of Physical Oceanography*, *13*(10), 1894–1907. https://doi.org/10.1175/1520-0485(1983)013<1894:UOHBDT>2.0.CO;2

Xie, S.-P., Deser, C., Vecchi, G. A., Ma, J., Teng, H., & Wittenberg, A. T. (2010). Global warming pattern formation: Sea surface temperature and rainfall. *Journal of Climate*, *23*(4), 966–986. https://doi.org/10.1175/2009JCLI3329.1

Yeh, S.-W., Ham, Y.-G., & Lee, J.-Y. (2012). Changes in the tropical Pacific SST trend from CMIP3 to CMIP5 and its implication of ENSO. *Journal of Climate*, *25*(21), 7764–7771. https://doi.org/10.1175/jcli-d-12-00304.1

Yu, J.-Y., Kao, P.-K., Paek, H., Hsu, H.-H., Hung, C.-w., Lu, M.-M., & An, S.-I. (2015). Linking emergence of the Central Pacific El Niño to the Atlantic multidecadal oscillation. *Journal of Climate*, *28*(2), 651–662. https://doi.org/10.1175/JCLI-D-14-00347.1

Yu, Z., & Schopf, P. S. (1997). Vertical eddy mixing in the tropical upper ocean: Its influence on zonal currents. *Journal of Physical Oceanography*, *27*(7), 1447–1458. https://doi.org/10.1175/1520-0485(1997)027<1447:vemitt>2.0.co;2

Zhang, C. (2001). Intraseasonal perturbations in sea surface temperatures of the equatorial eastern Pacific and their association with the Madden–Julian oscillation. *Journal of Climate*, *14*(6), 1309–1322. https://doi.org/10.1175/1520-0442(2001)014<1309:ipisst>2.0.co;2

Zuo, H., Balmaseda, M. A., Tietsche, S., Mogensen, K., & Mayer, M. (2019). The ECMWF operational ensemble reanalysis–analysis system for ocean and sea ice: A description of the system and assessment. *Ocean Science*, *15*(3), 779–808. https://doi.org/10.5194/os-15-779-2019